Electrochemical Charging of CdSe Quantum Dot Films: Dependence on Void Size and Counterion Proximity

Simon C. Boehme,[†,§] Hai Wang,[†,⊥,§] Laurens D.A. Siebbeles,[†] Daniel Vanmaekelbergh,[‡] and Arjan J. Houtepen[†,*]

[†]Chemical Engineering, Optoelectronic Materials, TU Delft, Julianalaan 136, 2628 BL Delft, The Netherlands and [‡]Debye Institute, Condensed Matter and Interfaces, Utrecht University, P.O. Box 80.000, 3508 TA Utrecht, The Netherlands. [§]S.C.B. and H.W. contributed equally to this work. [⊥]Present address: H.W.: Max Planck Institute for Polymer Research, Ackermannweg 1055128 Mainz, Germany.

ABSTRACT Films of colloidal quantum dots (QDs) show great promise for application in optoelectronic devices. Great advances have been made in recent years in designing efficient QD solar cells and LEDs. A very important aspect in the design of devices based on QD films is the knowledge of their absolute energy levels. Unfortunately, reported energy levels vary markedly depending on the employed measurement technique and the environment of the sample. In this report, we determine absolute energy levels of QD films by electrochemical charge injection. The concomitant change in optical absorption of the film allows quantification of the number of charges in quantum-confined levels and thereby their energetic position. We show here that the size of voids in the QD films (*i.e.*, the space between the quantum dots) determines the amount of charges that may be injected into the films. This effect is attributed to size exclusion of countercharges from the electrolyte solution. Further, the energy of the QD levels depends on subtle changes in the QD film and the supporting electrolyte: the size of the cation and the QD ligand length. These nontrivial effects can be explained by the proximity of the cation to the QD surface and a concomitant lowering of the electrochemical potential. Our findings help explain the wide range of reported values for QD energy levels and redefine the limit of applicability of electrochemical measurements on QD films. Finally, the finding that the energy of QD levels depends on ligand length and counterion size may be exploited in optimized designs of QD sensitized solar cells.

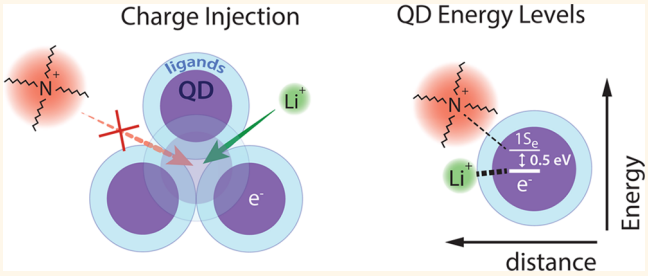

KEYWORDS: spectroelectrochemistry · electrochemical charging · quantum dot · surface functionalization · layer by layer · ligand · energy level

Colloidal quantum dot (QD) solids are promising for cost- and energy-efficient light harvesting, detection, and generation due to their tunable bandgap, solution processability,[1] stability,[2,3] and anticipated cost-efficiency.[4,5] Encouraging device efficiencies have been achieved in the fields of photovoltaics,[1,4,6,7] LEDs,[8−10] and (IR) photodetectors.[11] A compelling strategy to improve their luminescence (for LEDs) and charge extraction properties (for photovoltaics and photodetectors) is the implementation of a heterostructure consisting of two different semiconductor materials: by tuning the energy levels at either side, both the direction and rate of charge transfer can be controlled. However, the measurement of absolute energy levels (*vs* vacuum) remains a challenge. While a variety of experimental techniques is available, each one has its own pitfalls: ultraviolet photoelectron spectroscopy (UPS) can only determine energy levels of samples in vacuum[12] and photoelectron spectroscopy in air (PESA) only of samples in air.[13] Whereas the former measurement may be irrelevant for an actual device configuration, the latter has to cope with the poor stability of QDs in air. In addition, both are intrinsically limited to the surface of the film. This drawback is shared by Kelvin probe measurements.[14] Finally, electrochemistry can determine energy levels of the entire volume of a sample and under a variety of dielectric environments.[15] However, the commonly employed cyclic voltammetry measurement mode (CV) per definition cannot distinguish between QD levels and

* Address correspondence to A.J.Houtepen@tudelft.nl.

Received for review December 18, 2012 and accepted February 11, 2013.

Published online February 11, 2013
10.1021/nn3058455

defect states resulting from impurities or the surface of a QD. Since surface defects are abundant and very sensitive to a sample's preparation conditions and history, CV measurements often feature a large sample-to-sample variation and their interpretation is difficult. Hence, it is not surprising that the spread in literature values for energy levels determined by CV measurements surpasses 1.5 V. This discourages any effort to improve the performance of a working device *via* careful fine-tuning of its energy level alignment based on the existing literature of energy levels.

On the other hand, *spectro*-electrochemistry adds to the reliability of electrochemical energy level studies since it simultaneously probes changes in transmission and/or luminescence as a function of the applied potential to the sample. This way, it is possible to unambiguously distinguish charges in (optically active) QD orbitals from charges in defect states.[15−20] Such "electrolyte gating" (also called "electrochemical gating")[15] has been successfully exploited by several groups to study absolute energy levels,[18] investigate charge associated absorption changes and fluorescence quenching,[19,21] blinking characteristics,[22,23] or induce order-of-magnitude increases in steady-state conductivities.[20,24]

One reason for the success of the above spectroelectrochemical studies roots in the nanoporous morphology of a QD film: simultaneous with the injection of electrons or holes into the QD film, electrolyte counterions (present in the voids of the films) allow for a nanoscale charge compensation. Hence, while only the surface of a macroscopic semiconductor crystal can be charged, it is possible to charge the complete "bulk" volume of a QD film. Furthermore, one would expect that the type of counterion has little influence on the efficiency and energy of charging the QD film as long as the counterions are electrochemically inactive.

In this report, we determine the absolute energies of the $1S_e$ and $1P_e$ electron levels in CdSe QD films by spectroelectrochemistry. In particular, the spotlight is moved to charge injection in QD films whose conductivities are increased *via* reduced interparticle spacing by short cross-linking molecules, that is, the ligands. We find that in those films the maximum number of injectable electrons is limited by the size of the film's voids. The latter can be tuned *via* the diameter of the QDs and the length of the ligands that separate them. Furthermore, we report two peculiar observations concerning the absolute electron energy levels: (1) they depend on the cation size; this is not expected given the assumption that the cation is electrochemically inactive (see above). (2) They depend on the length of the QD ligand; this is not expected as a recent report finds energy level shifts due to the binding group of a linker, but not its length.[13] Both observations suggest that the cation tends to approach the QDs as close as possible, and that the proximity of the cations and the negatively charged QDs is an important factor in the overall energy of the system.

RESULTS AND DISCUSSION

QDs with diameters ranging from 2.4 to 8 nm were synthesized following the procedure by Mekis *et al.*[25] QD films were grown on ITO (indium tin oxide) substrates with a layer-by-layer (LbL) dipcoating method in a N_2 purged glovebox. Charge injection into CdSe QD films was investigated using a spectroelectrochemical setup in which the sample's substrate served as the working electrode in a three-electrode electrochemical cell (see Figure 1a). The Fermi level of the QD film is raised by a negative voltage between the sample's substrate and the Ag wire pseudoreference electrode (see Figure 1b). The resulting injection of electrons in the QD film and simultaneous charge compensation by cations in the electrolyte is monitored by a change in

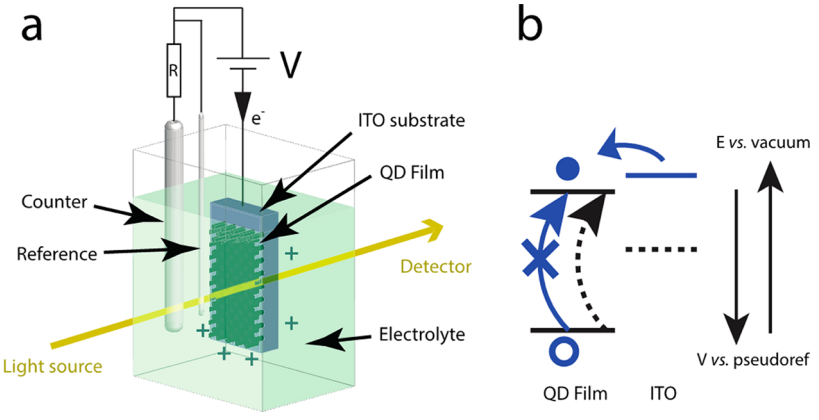

Figure 1. (a) Schematic of the spectroelectrochemical setup: *via* the potentiostat a voltage is applied between the Ag wire pseudoreference electrode and the QD film on an ITO substrate, both of which are immersed in the supporting electrolyte. Simultaneously, the electrochemical charging current is measured by a counter electrode and the change in the QD film absorption is monitored by a UV−vis spectrometer. (b) Schematic of the electron injection process: raising the Fermi level of the ITO from within the QD bandgap (black dashed line) to above the bandgap (blue continuous line) allows electron injection into an electronic level of the QD film. This blocks transitions to this level and thereby bleaches the absorption.

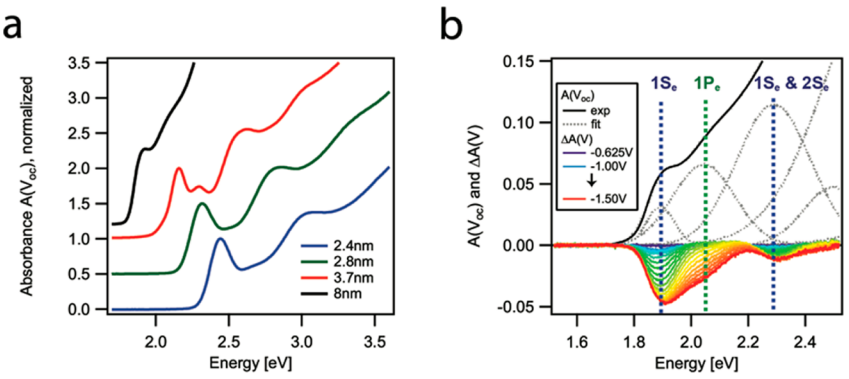

Figure 2. (a) Normalized absorption spectra $A(V_{oc})$ of QD dispersions with diameters ranging from 2.4 to 8 nm. For clarity, the spectra are offset vertically. (b) The absorption spectrum $A(V_{oc})$ of a 8DA-linked film of 8 nm QDs (black continuous line) can be fitted by multiple Gaussians (black dashed lines). Starting from about −1 V *vs* the Ag pseudoreference electrode, the QD film gets reduced inducing an absorption bleach $\Delta A(V)$ of these transitions. The involved electron levels are indicated by vertical dashed lines. The supporting electrolyte is 0.1 M $LiClO_4$ in anhydrous acetonitrile.

the absorption of the QD film. See Methods section for details.

Known size confinement effects such as an increase of the bandgap and discretization of electronic states are observed in an absorbance measurement $A(V_{oc})$ of our QD dispersions of five different diameters, at open circuit potential V_{oc} (see Figure 2a). Compared to the spectrum of the original dispersion, the QD films with 1,2-ethanediamine (2DA), 1,4-butanediamine (4DA), 1,6-hexanediamine (6DA), and 1,8-octanediamine (8DA) show a minor redshift and some broadening of the lowest energy transition (see Supporting Information). In Figure 2b, the spectrum of a 8DA-linked film of 8 nm QDs is fitted by multiple Gaussians in the energy region between 1.65 and 3.45 eV to unveil the underlying optical transitions. Following Norris and Bawendi,[26] the first Gaussian can be assigned to the nearly overlapping $1S_{3/2}1S_e$ and $2S_{3/2}1S_e$ transitions at 1.9 eV, the second Gaussian can be ascribed to the $1P_{3/2}1P_e$ transition at 2.05 eV and the third Gaussian may originate from the $3S_{3/2}1S_e$, $1S_{1/2}2S_e$, and $4S_{3/2}2S_e$ transitions at 2.3 eV. The relatively large size of the QDs precludes a more detailed assignment of transitions.

Determination of $1S_e$ and $1P_e$ Energy Levels. We now endeavor to determine the absolute energy of the confined electron levels for some of the observed transitions. Upon applying a negative potential on the sample's substrate (in case of a conductive film equivalent to shifting the Fermi level of both substrate and sample toward vacuum), we witness a negative change in the film's absorption (see Figure 2b) compared to the absorption at open circuit $A(V_{oc})$. This probe energy and potential dependent absorption bleach $\Delta A \equiv A(V) - A(V_{oc})$ is seen at the lowest energy transitions. At about −1 V *vs* the Ag wire pseudoreference potential, first the transitions involving the $1S_e$ electron level start to bleach and disappear completely at about −1.5 V, whereas from about −1.2 V also the transitions involving the $1P_e$ level start to bleach. To distinguish the contributions of both electron levels, we identify several Gaussian transitions in the potential dependent spectra, as for the ground state spectrum. We classify them by their involved electron levels such that $A_i(V)$ is the absorption resulting from all transitions involving the level i ($i = 1S_e, 1P_e, \ldots$) and $\Delta A_i(V)$ the respective absorption bleach. In Figure 2b, the spectra $A_i(V_{oc})$ are shown as black dashed lines and the involved levels i are indicated by vertical dashed lines.

The number of charges injected into a QD energy level i ($i = 1S_e, 1P_e, \ldots$) can be determined[24,27] from

$$\langle n_{\mathrm{opt},i}(V)\rangle = g_i \int_{E_L}^{E_U} \Delta A_i(E,V)/A_i(E,V_{oc})\,\mathrm{d}E \qquad (1)$$

where $\langle n_{\mathrm{opt},i}(V)\rangle$ is the average number of electrons per QD in level i at an applied potential V, g_i the degeneracy of this level and E_L and E_U the lower and upper bound of the energy interval, respectively. We choose E_L = 1.4 eV and E_U = 3.0 eV as the lower and upper bound, respectively. This choice is based on experimental limitations, however justified by the saturation of the integral within the chosen interval: for all of the samples, the integral stays constant when shifting the bounds at either side. Consequently, $\langle n_{\mathrm{opt,tot}}(V)\rangle = \Sigma_i\langle n_{\mathrm{opt},i}(V)\rangle$ is then the average total number of electrons per QD in quantum confined levels. The main source of uncertainty in the determination of n lies in the accuracy of the Gaussian fit to the absorption spectra. For $n < 2$ this fit is quite accurate, as the first transition is found to saturate at 2 electrons per QD, as expected. For higher electron numbers the uncertainty increases and likely is of the order of 20%. In the following, we introduce two synonyms: "relative bleach" for $\Delta A_i(V)/A_i(V_{oc})$ and "differential (relative) bleach" for its discrete derivative $1/A_i(V_{oc})\cdot\Delta[\Delta A_i(V)/A_i(V_{oc})]$.

The incremental filling of electronic states in a QD film is illustrated in Figure 3 as the differential bleach $\Delta[\Delta A_i(V)]/\Delta V$ and the differential capacitance $\Delta Q(V)/\Delta V$. The former yields the density of optically active states

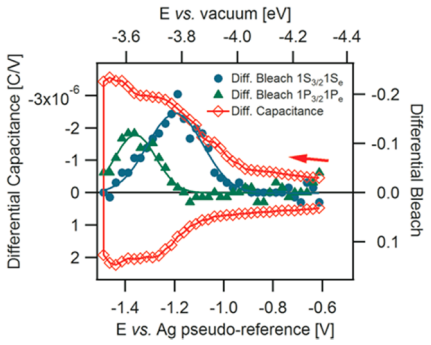

Figure 3. Determination of electron energy levels in a film of 8 nm CdSe QDs with 8DA ligands by means of differential capacitance $\Delta Q(V)/\Delta V$ (open diamonds) and differential absorption bleach $\Delta[\Delta A_i(V)]/\Delta V$ at transitions involving the $1S_e$ level (closed circles) and $1P_e$ level (closed triangles), respectively. Gaussian fits to the differential bleaches are displayed as continuous lines. The electrolyte is 0.1 M $LiClO_4$ in acetonitrile.

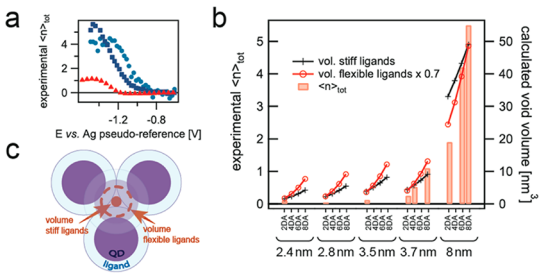

Figure 4. (a) Saturation of the number of electrons injected for films of 8 nm QDs with 6DA (circles) and 8DA ligands (squares), respectively, and a film of 3.7 nm QDs with 8DA ligands (triangles). (b) Experimentally determined maximum number of electrons per QD $\langle n_{tot}\rangle$ (bars) and calculated void volume assuming stiff ligands (line with crosses) and flexible ligands (line with open circles), respectively, as explained in the text. The films are categorized by their QD diameter and their ligand length, the latter ranging from two (2DA) to eight (8DA) C atoms. The supporting electrolyte is 0.1 M $LiCLO_4$ in acetonitrile. (c) Schematic of a tetrahedral void in the hard sphere model. The fourth and out-of-plane QD is half-transparent, the calculated void volume for stiff and flexible ligands is indicated by a filled and dashed circle, respectively.

$\Delta\langle n_{opt,i}\rangle/\Delta V$ according to eq 1, while the latter relates to the "electrochemical" DOS $\Delta\langle n_{ec}\rangle/\Delta V = (\Delta Q(V)/\Delta V)/(eN)$ where $\langle n_{ec}\rangle$ is the average number of electrons injected into the film per QD, e is the elementary charge, and N is the number of QDs in the film. This "electrochemical" DOS[28] includes optically dark electrons which may reside, for instance, in surface states. Hence, if the only charging that occurs is charging of the QD energy levels, the differential optical bleach and the differential capacitance should rise simultaneously with decreasing voltage. Indeed, the first wave in the differential capacitance (open diamonds in Figure 3) clearly coincides with filling of $1S_e$ electron levels (closed circles), whereas the second wave in the differential capacitance is related to charging of $1P_e$ states (closed triangles). We can thus conclude that within the observed time window (see Supporting Information) there is negligible charging of states other than the quantum confined ones.

The reversible charging and discharging of QD films hence enables the observation of quantum size confinement both optically and electrochemically. First, in the case of 8 nm QDs, we find the $1S_e$ and $1P_e$ levels to reside at −3.80 and −3.65 eV *vs* vacuum (or at −1.20 and −1.35 V *vs* the Ag pseudoreference electrode, respectively), as inferred from the extrema in the Gaussian fits to the differential bleach. This experimentally determined $1S_e-1P_e$ intraband separation of 0.15 eV is close to the expected intraband separation based on photoluminescence excitation data of Norris and Bawendi:[26] their reported difference of 0.15 eV between the $1S_{3/2}1S_e$ and $1P_{3/2}1P_e$ transition translates into a $1S_e-1P_e$ intraband separation of 0.11 eV, using effective masses of $0.13m_0$ and $0.44m_0$ for electron and hole, respectively. It also agrees with the infrared absorption data of smaller QDs in solution: the reported $1S_e-1P_e$ intraband separation of QDs with diameters between 2.7 and 5.4 nm ranges from 0.27 to 0.5 eV.[18] Second, we find that in films of 3.7 nm QDs the injection into $1S_e$ electron orbitals occurs at a 0.16 eV higher potential than in films of 8 nm QDs (see Supporting Information). This is in coarse agreement with the 0.21 eV offset expected from the 0.27 eV larger confinement energy (see Figure 2a) and the above electron and hole effective masses.

Void Size Limited Electron Injection. Using eq 1 we have determined the average number of electrons per QD $\langle n_{tot}\rangle$ for various QD diameters and diamine ligand lengths. Figure 4a shows $\langle n_{tot}\rangle$ *vs* applied potential for three films in a 0.1 M $LiClO_4$ electrolyte: 3.7 nm QDs and 8DA ligands (triangles), 8 nm QDs with 6DA (circles), and 8DA ligands (squares). For all films the number of injected charges is found to saturate at a certain potential: applying a more negative potential does not result in additional injection of electrons into the QD energy levels. The value of $\langle n_{tot}\rangle$ at which this saturation occurs varies for the different films. For the 8 nm QD diameter film with 8DA ligands the maximum occupation of quantum confined electron levels is 5.5 electrons per QD. However, reducing either QD diameter (from 8 to 2.4 nm) or ligand length (from 8DA = octanediamine to 2DA = ethanediamine) results in fewer electrons injected (see Figure 4b). We hypothesize that the maximum number of injected electrons per QD is limited by the size of the film's voids. We hereby assume that the ligand length controls the inter-QD separation. This has been shown by several authors, including our group, by X-ray scattering[29] and electron microscopy[30] as well as conductivity measurements.[31,32] Consequently, in the case of very small voids, that is, for densely packed films cross-linked *via* 2DA, insufficient cation compensation permits charging only at the surface of the entire film.

This situation is equivalent to charging of a *planar* semiconductor: the potential drops in the depletion region where charging is possible.[15] The bulk of the film remains uncharged. In this picture, efficient charge injection requires voids to be large enough for hosting electrolyte cations, as is the case in the films of large QDs with long ligands.

Hard Sphere Model. To test this hypothesis, in the following, we estimate the sizes of both the cations and the voids. The sizes of the former can be found in literature and range from 0.5 nm (*i.e.*, Li^+, solvated by acetonitrile molecules)[33] to 0.93 nm (*i.e.*, TOA^+, "solvated" by its alkyl chains),[34] the sizes of the latter are calculated in a hard sphere model. Herein, the QDs are modeled by hard spheres forming a closed-packed fcc lattice, as Murray *et al.*[35] have found evidence of fcc stacking in self-assembled CdSe QD lattices. We assume that the available void volume for uptake of electrolyte cations is given by the largest possible spheres that fit in the octahedral and tetrahedral voids of this stack. For N ligand-free QDs of radius R, there are N octahedral and $2N$ tetrahedral voids of radii 0.414 and 0.225 R, respectively.[36] Owing to the ligands on the QDs, the volume of both voids is enlarged, as sketched in the two scenarios in Figure 4c: either the ligands are assumed "stiff", in which case they merely increase the apparent radius R of the QD, or they are "flexible" in the sense that they permit full penetration of electrolyte ions and could thus be seen as a solvent that increases the distance between QDs. In Figure 4c, a tetrahedral void in the stiff case is sketched as a filled orange circle, a void in the flexible case is sketched as a dashed orange circle. The combined volume of the one octahedral void and the two tetrahedral voids per QD for ligands of length l can then be calculated as $V_{\mathrm{stiff,tot}} = {}^4/_3\pi[(0.414(R+l))^3 + 2(0.225(R+l))^3]$ in the case of stiff ligands and $V_{\mathrm{flex\ tot}} = {}^4/_3\pi[(0.414\cdot(R+l)+l)^3 + 2(0.225(R+l)+l)^3]$ in the case of flexible ligands, respectively. Both calculated volumes are shown in Figure 4b for different QD diameters and various ligands. The increase in the calculated void volume qualitatively agrees with the trend observed in the experimentally determined average electron occupation $\langle n_{\mathrm{tot}}\rangle$ per QD. This shows that if there is more volume available for cation uptake (in the case of large QDs and long ligands), more electrons can be injected into the QDs.

The qualitative agreement of the hard sphere model with the measured average electron occupation $\langle n_{\mathrm{tot}}\rangle$ is remarkable given the crude assumptions of the model. Specifically, our films will not be as ordered as assumed in the above hard sphere model. It is known that dipcoating results in glassy, rather than ordered films.[37,38] Furthermore, we so far neglected any interaction between injected electrons and electrolyte cations. For high degrees of charging with multiple cations per void as observed in the films with 8 nm QDs and long 8DA ligands, this should lead to deviations from our hard sphere model.

Summarizing, we show here that the small interparticle spacing of highly conductive QD films necessarily limits their electrochemical charging ability. This is in line with a puzzle presented in an earlier report:[39] CdSe QD films treated with NaOH were found to be chargeable up to a concentration that amounts to charging of the first monolayer at the surface of the film. Exposure to NaOH effectively removes all ligands leaving OH^- at the surface.[40] We suggest that in this case the voids in the film have been too small for cation uptake. The importance of nanoporosity for efficient charging has also been demonstrated in a recent study on graphene based electrochemical capacitors:[41] increasing the porosity in graphene layers was the recipe to achieve capacitors of both high power density and high energy density.

Ligand Length and Cation Size. In the following we want to address the *energetics* of electron injection in CdSe QD films. As outlined above, we draw our motivation from the large spread in reported values for QD electron energy levels. Figure 5a shows the potential dependent charging of films of 8 nm QDs with ligands of varying length. For the 6DA and 8DA ligands, the relative bleach of the $1S_{3/2}1S_e$ transition saturates at $\sim$1, indicating full (2-fold) charging of the $1S_e$ level. This is in line with the conclusion above that in these films in total more than four or five electrons per QD can be injected, respectively. However, for the shorter 6DA ligands we observe a $\sim$ 200 meV lower injection potential (defined as the minimum of the differential relative bleach). While for the 2DA ligands the incomplete relative bleach at saturation due to reduced void size precludes a quantification of the shift, the high relative bleach at low potentials for 2DA ligands confirms the trend that electron injection occurs at lower potential when the ligand length is decreased. The same qualitative trend of a lowering of the injection potential also holds for films of 3.7 nm diameter QDs (see Supporting Information).

While it is conceivable that the ligand itself causes a shift of the energetic position of the QD electron levels, a recent study using photoelectron spectroscopy in air (PESA) showed only negligible variations in the energy levels for films of QDs with varying length of the amine capping.[13] We therefore hypothesize that the distance between cation and injected electron in the QD determines the injection potential instead: an increased proximity of the charges on cation and QD imposes an attractive Coulomb interaction, thereby lowering the electrochemical potential of injection.

To corroborate this hypothesis, we also varied the cation size, with $Li^+ < TBA^+ < TOA^+$.[33,42] Figure 5c displays the charging of a film with 8 nm QDs and 8DA ligands. The large void size in this film allows facile counterion penetration, even in case of the largest ion

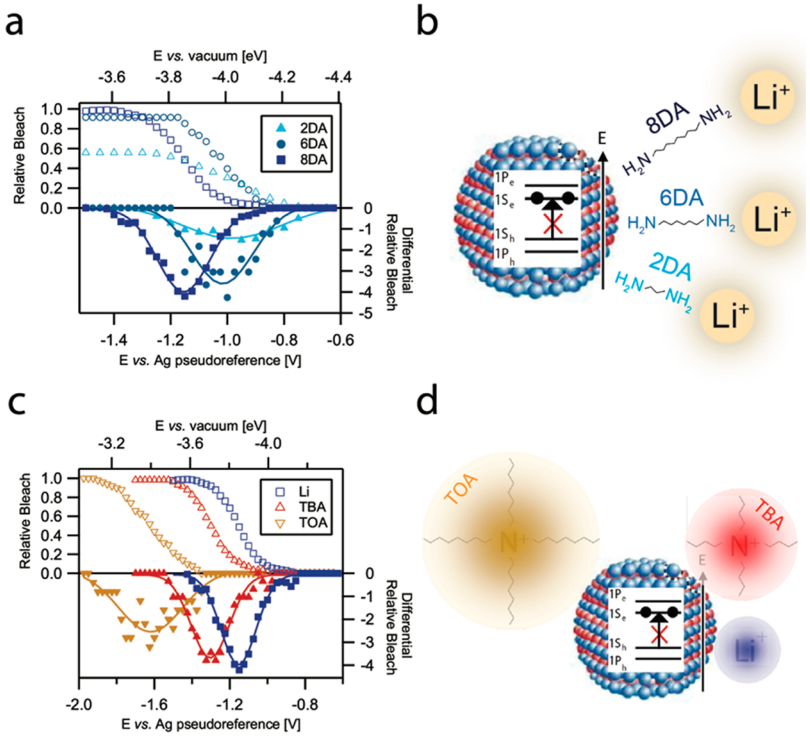

Figure 5. (a) Potential dependence of the relative bleach at the $1S_{3/2}1S_e$ transition (open symbols) and the differential relative bleach at this transition (closed symbols) for films of 8 nm QDs cross-linked with 2DA (triangles), 6DA (circles), or 8DA (squares), respectively. Gaussian fits to the differential relative bleaches are shown as continuous lines. (b) Schematic illustrating increased proximity of cation and QD for decreasing ligand length. Note that the QDs, ligands, and Li+ ions are not sketched with their true relative size. (c) Bleaching of a 8DA-linked film of 8 nm QDs in acetonitrile electrolytes using cations of increasing size: from Li+ (squares) to TBA+ (upward triangles) to TOA+ (downward triangles). (d) Schematic illustrating the different sizes of used electrolyte cations. Note that the QDs and ions are not sketched with their true relative size.

TOA^+. This is evident from the complete bleach of the $1S_{3/2}1S_e$ transition for all cations used. We observe a lowering of the injection potential by 500 meV when the size of the cation reduces from TOA^+ to TBA^+ to Li^+. This is consistent with the above proposed scenario in which the proximity of the charges on cation and QD lowers the electrochemical potential of injection.

Comparison to Ionic Lattices. One might compare the charged QD film to an ionic lattice comprising negative charges (being the electrons in the QD film) and positive charges (being the electrolyte cations in the voids of the QD film). One could assume that, as is the case for atomic ionic lattices, the cations sit symmetrically between the QDs in the center of the voids. As a result, the total potential of the lattice and, thus, the electrochemical potential of electron injection, should only slightly depend on the ligand length (due to lattice contraction, see Supporting Information) and should not depend on the size of the cation.

In strong contrast to this picture, Figure 5 panels a and c show that the injection potential is lowered by 200 meV due to a decrease in the ligand length and by 500 meV due to a decrease in cation size. Therefore, we suggest that, unlike cations in atomic ionic lattices, the cations in a film of QDs try to approach the charged QDs as close as possible. Their proximity to the QDs, and hence the film's potential, is controlled by the ligand length and the cation size: the ligand acts as a "spacer", increasing the film's potential with increasing ligand length; the cation size leads to the same effect by controlling the proximity of the charge on the ion and the electron on the QD *via* the thickness of the ion's solvation shell (in case of Li^+) or the length of its alkyl side chain (in case of TBA^+ and TOA^+), respectively.

Apparently cations in QD films do not behave like cations in ionic lattices. This can be understood when we consider that in atomic ionic lattices steric hindrance is responsible for locating the cations in the center of a void. The size ratio between cations and anions is much larger (~1:1) than the QD/cation size ratio. The similarity of the ionic radii of anions and cations immobilizes the cations in the (center of the) small voids of the anionic sublattice. In QD lattices, however, the large ratio in size of QD and cation creates voids that are larger than the cation and permit the cation to "move".

Voids in real films are even larger, since dipcoating results in glassy, rather than ordered films.[37,38] Disorder gives rise to inclusions of large voids where the electrochemical potential of electron injection will be controlled by the ligand length and cation size, as they determine the distance between electron and cation (see Figure 5). This situation is similar to the charging of

a planar semiconductor. Hence, the charged QD film can be modeled by specific optimized electron/cation pairs and absence of ion-lattice periodicity.

Similarly, mesoporous oxide films in dye or QD sensitized solar cells feature larger voids (a few to a few tens of nanometers) and their conduction band minima were found to shift substantially with surface functionalization.[43−46] Apparently, both the mesoporous oxide films and our CdSe QD film compare better to a planar bulk semiconductor than to atomic ionic lattices. Studies on dye sensitized solar cells already paid substantial attention to the choice of the electrolyte: charge transfer rates could be influenced[47−49] and the overall device performance optimized[43,50] solely by the choice of the electrolyte salt and its concentration. It was found that the conduction band position of metal oxide particles and thus the open circuit voltage mainly depends on the charge-to-size ratio of the electrolyte cation. Specifically, an increasing concentration of Li^+ led to significant shifts of the metal oxide conduction band edge away from vacuum, lowering the V_{oc}.[44−46] In general, this trend pronounces with increasing cationic charge-to-radius ratio and decreasing pH.[43−45] The underlying origin of the positive shifts for small cations continues to stimulate debate with explanations put forward ranging from a reduced distance between charges of opposite sign[44] to facilitated cation intercalation into the sample's lattice.[45,51−57]

We find a similar trend in our spectroelectrochemical study on CdSe QD films: in the case of sufficiently large QDs, a decrease of the ligand length or a decrease of the cation size lowers the electrochemical potential for electron injection into the discrete levels. This is consistent with enhanced Coulomb attraction between electron and cation. Thus, the proximity between injected electron in the QD and cation in the void determines the electronic energy level. This finding sheds light on the origin of the present spread in literature values for one and the same QD electron energy level. The sensitivity of the electrochemical potentials to QD ligands and electrolyte composition should be borne in mind when using electrochemistry to determine absolute energy levels in conductive QD films. In such measurements, the motivation for using small cations and long ligands is 2-fold: (1) the necessary porosity for introducing cations is given and (2) the ligands act as "spacers" keeping the cations at a distance, thereby allowing less perturbation of the film's energy levels by cations themselves. However, the choice of both the ligand and the electrolyte also allows control of absolute energy levels in QD films. In QD sensitized solar cells in particular, this can be exploited when engineering the free energy difference between injecting QD electron level and the metal oxide conduction band to optimize the short-circuit current J_{sc} and open circuit voltage V_{oc} of the device.

CONCLUSIONS

We report electrochemical charge injection of up to 5.5 electrons per QD, yielding the absolute energetic position of both $1S_e$ and $1P_e$ electron levels in CdSe QD films. The maximum electron occupation in quantum-confined states is limited by the uptake of charge compensating electrolyte cations. We identify the physical size of film voids as the main bottleneck, resulting in efficient charging for large QDs with long ligands and small electrolyte cations. Furthermore, the potential of the $1S_e$ energy level shifts away from vacuum if (1) quantum confinement decreases or if the distance between cation and QD decreases due to (2) small cations or (3) decreased length of the QD ligand. Such influence of the film morphology, surface functionalization as well as the electrolyte composition on the QD energy levels must not be neglected in electrochemical measurements of QD films. On the other hand, spectroelectrochemistry serves as a tool to sense and control electrostatic interactions with the electrolyte, illuminating the route toward an optimized design of future optoelectronic devices such as QD sensitized solar cells.

METHODS

QD Synthesis. QDs were synthesized following Mekis *et al.*:[25] two precursors were prepared in a N_2 purged glovebox by dissolving 0.474 g of Se (325 mesh) in 6 mL of TOP (trioctylphosphine) and 0.36 g of $Cd(Ac)_2$ in 9 mL of TOP, respectively. An amount of 24 g of TOPO (trioctylphosphine oxide) was heated to 180 °C in vacuum under periodic flushing with N_2. After cooling down to 100 °C, 15g of HDA (1-hexadecylamine) and 0.45 g of TDPA (1-tetradecylphosphonic acid) were added and dried at 120 °C in vacuum during 30 min under periodic flushing with N_2. The TOP−Se precursor was injected and the solution was heated to 300 °C under N_2 flow. Under vigorous stirring, the TOP−$Cd(Ac)_2$ precursor was injected to induce nucleation of CdSe nanoparticles. During the growth at 280 °C, aliquots were taken to monitor the growth rate. After the desired QD size was reached, the reaction was stopped by cooling down to room temperature. Toluene was injected to avoid solidification of the TOPO. The obtained dispersion was purified by repeated washing with MeOH and precipitation of particles in a centrifuge at 3000 rpm for 5 min. The final stock of particles was dispersed in chloroform.

QD Film Processing by LbL Dipcoating Procedure. QD films were grown in a layer-by-layer (LbL) dipcoating procedure in a N_2 purged glovebox. ITO (indium tin oxide) substrates were first immersed for 30 s in a concentrated QD dispersion, subsequently immersed for 30 s in a stirred MeOH solution containing 10 vol % of the desired ligand and finally rinsed by residing 60 s in stirred MeOH. Using this procedure, the original insulating ligands are replaced by the new desired ligand. Typically, the above procedure was repeated 20 times to yield films roughly 20 QD monolayers thick. After dipcoating, the film was kept on a hot plate at 70 °C to evaporate residual solvent. For all the films, a small region on the edge of the substrate remained uncoated for contacting in electrochemical measurements.

Spectroelectrochemical Measurements. Our electrochemical setup consists of a CHI832B bipotentiostat (CH Instruments, Inc.) with an Ag wire pseudoreference electrode and a Pt sheet counter electrode in an airtight Teflon container (see Figure 1a). The Ag wire pseudoreference electrode (−5.00 V *vs* vacuum) was calibrated with a ferrocene/ferrocinium couple (see Supporting Information)[58,59] In a N_2 purged glovebox, the cell is loaded with a QD film and filled with an electrolytes consisting of anhydrous acetonitrile (≥99.8%, Sigma-Aldrich) and either 0.1 M $LiClO_4$ (lithium perchlorate, battery grade, 99.99%, Aldrich), 0.1 M $TBAPF_6$ (tetrabutylammonium hexafluorophosphate, ≥ 99.0%, Fluka), or 0.1 M $TOABF_4$ (tetraoctylammonium tetrafluoroborate, ≥ 97.0%, Aldrich). All chemicals were used as received.

We perform electrochemical measurements in the so-called "differential capacitance" mode.[15,60] The charging current is integrated during a fixed time interval following a potential step yielding the differential capacitance, that is, the injected charge per potential step $\Delta Q/\Delta V$. This removes the contribution of faradaic background currents in the electrolyte. Second, the electric double layer capacitance can be corrected for by a separate differential capacitance measurement of a bare ITO substrate. The so obtained differential capacitance of the QD film then reveals the sample characteristic charging and discharging features much more clearly than common CV measurements (see Supporting Information). On the basis of sample-to-sample variations, we estimate a 50 meV error in the reported potentials.

In the same experimental setup, UV−vis absorption measurements are performed using a HL-2000 halogen lamp (Ocean Optics) and a USB2000+ spectrometer (Ocean Optics). After passing through the electrochemical cell *via* two windows in the Teflon container, the light is collected in an optical fiber and its intensity is adjusted by a diaphragm and collimating lenses. The absorption bleach spectrum of each potential step is taken after the electrochemical current has decayed to a stable level.

Conflict of Interest: The authors declare no competing financial interest.

Acknowledgment. We thank T. Savenije, L. Kunneman and S. ten Cate for helpful discussions. This work is part of the Joint Solar Programme (JSP) of HyET Solar and the Stichting voor Fundamenteel Onderzoek der Materie (FOM), which is part of The Netherlands Organisation for Scientific Research (NWO).

Supporting Information Available: Absorption spectra of QD films and dispersions, cyclic voltammogramm, influence of film thickness, ligand dependence, cation dependence, calibration of pseudoreference electrode, charging energy. This material is available free of charge *via* the Internet at http://pubs.acs.org.

REFERENCES AND NOTES

1. Gur, I. Air-Stable All-Inorganic Nanocrystal Solar Cells Processed from Solution. *Science* **2005**, *310*, 1618–1618.
2. Luther, J. M.; Gao, J.; Lloyd, M. T.; Semonin, O. E.; Beard, M. C.; Nozik, A. J. Stability Assessment on a 3% Bilayer PbS/ZnO Quantum Dot Heterojunction Solar Cell. *Adv. Mater.* **2010**, *22*, 3704–3707.
3. Tang, J.; Wang, X.; Brzozowski, L.; Barkhouse, D. A. R.; Debnath, R.; Levina, L.; Sargent, E. H. Schottky Quantum Dot Solar Cells Stable in Air under Solar Illumination. *Adv. Mater.* **2010**, *22*, 1398–1402.
4. Sargent, E. H. Infrared Photovoltaics Made by Solution Processing. *Nat. Photonics* **2009**, *3*, 325–331.
5. Sargent, E. H. Colloidal Quantum Dot Solar Cells. *Nat. Photonics* **2012**, *6*, 133–135.
6. Tang, J.; Kemp, K. W.; Hoogland, S.; Jeong, K. S.; Liu, H.; Levina, L.; Furukawa, M.; Wang, X.; Debnath, R.; Cha, D.; *et al.* Colloidal-Quantum-Dot Photovoltaics Using Atomic-Ligand Passivation. *Nat. Mater.* **2011**, *10*, 765–771.
7. Ip, A. H.; Thon, S. M.; Hoogland, S.; Voznyy, O.; Zhitomirsky, D.; Debnath, R.; Levina, L.; Rollny, L. R.; Carey, G. H.; Fischer, A.; *et al.* Hybrid Passivated Colloidal Quantum Dot Solids. *Nat. Nanotechnol.* **2012**, *7*, 577–582.
8. Anikeeva, P. O.; Halpert, J. E.; Bawendi, M. G.; Bulović, V. Quantum Dot Light-Emitting Devices with Electroluminescence Tunable over the Entire Visible Spectrum. *Nano Lett.* **2009**, *9*, 2532–2536.
9. Zhang, Y.; Xie, C.; Su, H.; Liu, J.; Pickering, S.; Wang, Y.; Yu, W. W.; Wang, J.; Wang, Y.; Hahm, J.-i.; *et al.* Employing Heavy Metal-free Colloidal Quantum Dots in Solution-Processed White Light-Emitting Diodes. *Nano Lett.* **2011**, *11*, 329–332.
10. Sun, L.; Choi, J. J.; Stachnik, D.; Bartnik, A. C.; Hyun, B.-R.; Malliaras, G. G.; Hanrath, T.; Wise, F. W. Bright Infrared Quantum-Dot Light-Emitting Diodes through Inter-Dot Spacing Control. *Nat. Nanotechnol.* **2012**, *7*, 369–373.
11. Konstantatos, G.; Sargent, E. H. Nanostructured Materials for Photon Detection. *Nat. Nanotechnol.* **2010**, *5*, 391–400.
12. Munro, A. M.; Zacher, B.; Graham, A.; Armstrong, N. R. Photoemission Spectroscopy of Tethered CdSe Nanocrystals: Shifts in Ionization Potential and Local Vacuum Level as a Function of Nanocrystal Capping Ligand. *ACS Appl. Mater. Interfaces* **2010**, *2*, 863–869.
13. Jasieniak, J.; Califano, M.; Watkins, S. E. Size-Dependent Valence and Conduction Band-Edge Energies of Semiconductor Nanocrystals. *ACS Nano* **2011**, *5*, 5888–5902.
14. Gao, J.; Luther, J. M.; Semonin, O. E.; Ellingson, R. J.; Nozik, A. J.; Beard, M. C. Quantum Dot Size Dependent *J*−*V* Characteristics in Heterojunction Zno/Pbs Quantum Dot Solar Cells. *Nano Lett.* **2011**, *11*, 1002–1008.
15. Vanmaekelbergh, D.; Houtepen, A. J.; Kelly, J. J. Electrochemical Gating: A Method to Tune and Monitor the (Opto)Electronic Properties of Functional Materials. *Electrochim. Acta* **2007**, *53*, 1140–1149.
16. Guyot-Sionnest, P. Charging Colloidal Quantum Dots by Electrochemistry. *Microchim. Acta* **2008**, *160*, 309–314.
17. Guyot-Sionnest, P.; Wang, C. Fast Voltammetric and Electrochromic Response of Semiconductor Nanocrystal Thin Films. *J. Phys. Chem. B* **2003**, *107*, 7355–7359.
18. Shim, M.; Guyot-Sionnest, P. N-Type Colloidal Semiconductor Nanocrystals. *Nature* **2000**, *407*, 981–983.
19. Wang, C. J.; Shim, M.; Guyot-Sionnest, P. Electrochromic Nanocrystal Quantum Dots. *Science* **2001**, *291*, 2390–2392.
20. Yu, D.; Wang, C. J.; Guyot-Sionnest, P. N-Type Conducting Cdse Nanocrystal Solids. *Science* **2003**, *300*, 1277–1280.
21. Jha, P. P.; Guyot-Sionnest, P. Trion Decay in Colloidal Quantum Dots. *ACS Nano* **2009**, *3*, 1011–1015.
22. Galland, C.; Ghosh, Y.; Steinbruck, A.; Sykora, M.; Hollingsworth, J. A.; Klimov, V. I.; Htoon, H. Two Types of Luminescence Blinking Revealed by Spectroelectrochemistry of Single Quantum Dots. *Nature* **2011**, *479*, 203–207.
23. Jha, P. P.; Guyot-Sionnest, P. Electrochemical Switching of the Photoluminescence of Single Quantum Dots. *J. Phys. Chem. C* **2010**, *114*, 21138–21141.
24. Houtepen, A. J.; Kockmann, D.; Vanmaekelbergh, D. Reappraisal of Variable-Range Hopping in Quantum-Dot Solids. *Nano Lett.* **2008**, *8*, 3516–3520.
25. Mekis, I.; Talapin, D. V.; Kornowski, A.; Haase, M.; Weller, H. One-Pot Synthesis of Highly Luminescent CdSe/CdS Core−Shell Nanocrystals *via* Organometallic and "Greener" Chemical Approaches. *J. Phys. Chem. B* **2003**, *107*, 7454–7462.
26. Norris, D. J.; Bawendi, M. G. Measurement and Assignment of the Size-Dependent Optical Spectrum in CdSe Quantum Dots. *Phys. Rev. B* **1996**, *53*, 16338–16346.
27. Houtepen, A. J.; Vanmaekelbergh, D. Orbital Occupation in Electron-Charged CdSe Quantum-Dot Solids. *J. Phys. Chem. B* **2005**, *109*, 19634–19642.
28. Memming, R. *Experimental Techniques*; Wiley-VCH Verlag GmbH: 2007; p 61−80.
29. Choi, J. J.; Luria, J.; Hyun, B. R.; Bartnik, A. C.; Sun, L. F.; Lim, Y. F.; Marohn, J. A.; Wise, F. W.; Hanrath, T. Photogenerated Exciton Dissociation in Highly Coupled Lead Salt Nanocrystal Assemblies. *Nano Lett.* **2010**, *10*, 1805–1811.
30. Wolcott, A.; Doyeux, V.; Nelson, C. A.; Gearba, R.; Lei, K. W.; Yager, K. G.; Dolocan, A. D.; Williams, K.; Nguyen, D.; Zhu, X. Y. Anomalously Large Polarization Effect Responsible for Excitonic Red Shifts in PbSe Quantum Dot Solids. *J. Phys. Chem. Lett.* **2011**, *2*, 795–800.

31. Gao, Y.; Aerts, M.; Sandeep, C. S. S.; Talgorn, E.; Savenije, T. J.; Kinge, S.; Siebbeles, L. D. A.; Houtepen, A. J. Photoconductivity of PbSe Quantum-Dot Solids: Dependence on Ligand Anchor Group and Length. *ACS Nano* **2012**, *6*, 9606–9614.
32. Liu, Y.; Gibbs, M.; Puthussery, J.; Gaik, S.; Ihly, R.; Hillhouse, H. W.; Law, M. Dependence of Carrier Mobility on Nanocrystal Size and Ligand Length in PbSe Nanocrystal Solids. *Nano Lett.* **2010**, *10*, 1960–1969.
33. Spångberg, D.; Hermansson, K. The Solvation of Li+ and Na+ in Acetonitrile from *ab Initio*-Derived Many-Body Ion-Solvent Potentials. *Chem. Phys.* **2004**, *300*, 165–176.
34. Due to the high charge-to-radius ratio, Li^+ will have a solvation shell in acetonitrile. The radius of the solvated Li^+ was calculated by Spangberg *et al*. [ref 28] to be 0.5 nm. For TBA^+ and TOA^+ we neglect solvation shells, since their alkyl side chains may already provide sufficient solvation. The ion radii are then estimated from the length of the constituent bonds: 0.52 nm and 0.93 nm for TBA^+ and TOA^+, respectively.
35. Murray, C. B.; Kagan, C. R.; Bawendi, M. G. Synthesis and Characterization of Monodisperse Nanocrystals and Close-Packed Nanocrystal Assemblies. *Annu. Rev. Mater. Sci.* **2000**, *30*, 545–610.
36. Shriver, D.; Atkins, P. *Inorganic Chemistry*, 4th ed.; W. H. Freeman: Gordonsville, VA, **2006**.
37. Law, M.; Luther, J. M.; Song, Q.; Hughes, B. K.; Perkins, C. L.; Nozik, A. J. Structural, Optical, and Electrical Properties of PbSe Nanocrystal Solids Treated Thermally or with Simple Amines. *J. Am. Chem. Soc.* **2008**, *130*, 5974–5985.
38. Luther, J. M.; Law, M.; Song, Q.; Perkins, C. L.; Beard, M. C.; Nozik, A. J. Structural, Optical and Electrical Properties of Self-Assembled Films of PbSe Nanocrystals Treated with 1,2-Ethanedithiol. *ACS Nano* **2008**, *2*, 271–280.
39. Yu, D.; Wehrenberg, B. L.; Jha, P.; Ma, J.; Guyot-Sionnest, P. Electronic Transport of N-Type CdSe Quantum Dot Films: Effect of Film Treatment. *J. Appl. Phys.* **2006**, 99.
40. Nag, A.; Kovalenko, M. V.; Lee, J. S.; Liu, W. Y.; Spokoyny, B.; Talapin, D. V. Metal-Free Inorganic Ligands for Colloidal Nanocrystals: S(2−), HS(−), Se(2−), HSe(−), Te(2−), HTe(−), TeS(3)(2−), OH(−), and NH(2)(−) as Surface Ligands. *J. Am. Chem. Soc.* **2011**, *133*, 10612–10620.
41. El-Kady, M. F.; Strong, V.; Dubin, S.; Kaner, R. B. Laser Scribing of High-Performance and Flexible Graphene-Based Electrochemical Capacitors. *Science* **2012**, *335*, 1326–1330.
42. Memming, R. *Principles of Semiconductor Physics*; Wiley-VCH Verlag GmbH: 2007; p 1−21.
43. Haque, S. A.; Palomares, E.; Cho, B. M.; Green, A. N. M.; Hirata, N.; Klug, D. R.; Durrant, J. R. Charge Separation *versus* Recombination in Dye-Sensitized Nanocrystalline Solar Cells: The Minimization of Kinetic Redundancy. *J. Am. Chem. Soc.* **2005**, *127*, 3456–3462.
44. Morris, A. J.; Meyer, G. J. TiO_2 Surface Functionalization to Control the Density of States. *J. Phys. Chem. C* **2008**, *112*, 18224–18231.
45. Ardo, S.; Meyer, G. J. Photodriven Heterogeneous Charge Transfer with Transition-Metal Compounds Anchored to TiO_2 Semiconductor Surfaces. *Chem. Soc. Rev.* **2009**, *38*, 115–164.
46. Bisquert, J.; Fabregat-Santiago, F.; Mora-Seró, I.; Garcia-Belmonte, G.; Barea, E. M.; Palomares, E. A Review of Recent Results on Electrochemical Determination of the Density of Electronic States of Nanostructured Metal-Oxide Semiconductors and Organic Hole Conductors. *Inorg. Chim. Acta* **2008**, *361*, 684–698.
47. Pijpers, J. J. H.; Ulbricht, R.; Derossi, S.; Reek, J. N. H.; Bonn, M. Picosecond Electron Injection Dynamics in Dye-Sensitized Oxides in the Presence of Electrolyte. *J. Phys. Chem. C* **2011**, *115*, 2578–2584.
48. Koops, S. E.; O'Regan, B. C.; Barnes, P. R. F.; Durrant, J. R. Parameters Influencing the Efficiency of Electron Injection in Dye-Sensitized Solar Cells. *J. Am. Chem. Soc.* **2009**, *131*, 4808–4818.
49. O'Regan, B. C.; Durrant, J. R. Kinetic and Energetic Paradigms for Dye-Sensitized Solar Cells: Moving from the Ideal to the Real. *Acc. Chem. Res.* **2009**, *42*, 1799–1808.
50. Fabregat-Santiago, F.; Bisquert, J.; Garcia-Belmonte, G.; Boschloo, G.; Hagfeldt, A. Influence of Electrolyte in Transport and Recombination in Dye-Sensitized Solar Cells Studied by Impedance Spectroscopy. *Sol. Energy Mater. Sol. Cells* **2005**, *87*, 117–131.
51. Lemon, B. I.; Hupp, J. T. Electrochemical Quartz Crystal Microbalance Studies of Electron Addition at Nanocrystalline Tin Oxide/Water and Zinc Oxide/Water Interfaces: Evidence for Band-Edge-Determining Proton Uptake. *J. Phys. Chem. B* **1997**, *101*, 2426–2429.
52. Lyon, L. A.; Hupp, J. T. Energetics of Semiconductor Electrode/Solution Interfaces: EQCM Evidence for Charge-Compensating Cation Adsorption and Intercalation During Accumulation Layer Formation in the Titanium Dioxide/Acetonitrile System. *J. Phys. Chem.* **1995**, *99*, 15718–15720.
53. Van de Walle, C. G.; Neugebauer, J. Universal Alignment of Hydrogen Levels in Semiconductors, Insulators, and Solutions. *Nature* **2003**, *423*, 626–628.
54. Boschloo, G.; Fitzmaurice, D. Electron Accumulation in Nanostructured TiO_2 (Anatase) Electrodes. *J. Phys. Chem. B* **1999**, *103*, 7860–7868.
55. Kopidakis, N.; Benkstein, K. D.; van de Lagemaat, J.; Frank, A. J. Transport-Limited Recombination of Photocarriers in Dye-Sensitized Nanocrystalline TiO2 Solar Cells. *J. Phys. Chem. B* **2003**, *107*, 11307–11315.
56. Halverson, A. F.; Zhu, K.; Erslev, P. T.; Kim, J. Y.; Neale, N. R.; Frank, A. J. Perturbation of the Electron Transport Mechanism by Proton Intercalation in Nanoporous TiO_2 Films. *Nano Lett.* **2012**, *12*, 2112–2116.
57. Wei, D.; Scherer, M. R. J.; Bower, C.; Andrew, P.; Ryhänen, T.; Steiner, U. A Nanostructured Electrochromic Supercapacitor. *Nano Lett.* **2012**, *12*, 1857–1862.
58. Ruch, P. W.; Cericola, D.; Hahn, M.; Kötz, R.; Wokaun, A. On the Use of Activated Carbon as a Quasi-reference Electrode in Non-aqueous Electrolyte Solutions. *J. Electroanal. Chem.* **2009**, *636*, 128–131.
59. Wang, Y.; Rogers, E. I.; Compton, R. G. The Measurement of the Diffusion Coefficients of Ferrocene and Ferrocenium and Their Temperature Dependence in Acetonitrile Using Double Potential Step Microdisk Electrode Chronoamperometry. *J. Electroanal. Chem.* **2010**, *648*, 15–19.
60. Hulea, I. N.; Brom, H. B.; Houtepen, A. J.; Vanmaekelbergh, D.; Kelly, J. J.; Meulenkamp, E. A. Wide Energy-Window View on the Density of States and Hole Mobility in Poly(*p*-phenylene vinylene). *Phys. Rev. Lett.* **2004**, *93*, 166601.